Journal of Power Sources 245 (2014) 671–677

Contents lists available at SciVerse ScienceDirect

Journal of Power Sources

journal homepage: www.elsevier.com/locate/jpowsour

Fabrication and characterization of inert-substrate-supported tubular single cells by dip-coating process

Kai Zhao [a], Bok-Hee Kim [a,*], Qing Xu [b], Byung-Guk Ahn [a]

[a] Division of Advanced Materials Engineering, Hydrogen & Fuel Cell Research Center, Research Center of Advanced Materials Development, Chonbuk National University, Jeonbuk, Republic of Korea
[b] School of Materials Science and Engineering, Wuhan University of Technology, Wuhan, China

HIGHLIGHTS

- Inert yttria-stabilized zirconia supported tubular single cell is fabricated.
- Pore former amount in the supporter is a key technological parameter.
- An optimum maximum power density of 337 mW cm^{-2} is obtained at 800 °C in hydrogen.
- The cell maintains 95% of its initial performance within seven redox cycles.

ARTICLE INFO

Article history:
Received 27 May 2013
Received in revised form
2 July 2013
Accepted 3 July 2013
Available online 12 July 2013

Keywords:
Inert substrate supporter
Porous yttria-stabilized zirconia
Tubular single cell
Dip-coating
Cold isostatic pressing

ABSTRACT

A tubular single cell supported by an inert substrate with a configuration of porous yttria-stabilized zirconia (YSZ) supporter/Ni anode current collector/Ni–$Ce_{0.8}Sm_{0.2}O_{1.9}$ anode/YSZ/$Ce_{0.8}Sm_{0.2}O_{1.9}$ bi-layer electrolyte/$La_{0.6}Sr_{0.4}Co_{0.2}Fe_{0.8}O_{3-\delta}$ cathode has been fabricated by a cold isostatic pressing and dip-coating process. The effects of pore morphology and porosity of the YSZ supporter on the mechanical strength and electrochemical performance of the single cell have been investigated with respect to the content of poly (methyl methacrylate) (PMMA) pore former. The average pore size and porosity of the YSZ supporter increase with the amount of pore former used, facilitating the gas diffusion process at the anode and reducing the polarization resistance of the single cell whereas leading to a decline of the mechanical strength. A preferred pore former content is determined to be 25 wt.% based on a trade-off of the mechanical strength and electrochemical performance. The single cell with 25 wt.% PMMA in YSZ supporter shows a bending strength of 21 ± 1 MPa and a maximum power density of 337 mW cm^{-2} at 800 °C in hydrogen. Moreover, the inert-substrate-supported tubular single cell displays a satisfactory redox cycling stability, maintaining 95% of its initial performance within seven redox cycles.

1. Introduction

Solid oxide fuel cells (SOFCs) are energy conversion devices with high efficiency and environmental compatibility. The SOFCs operating at high temperatures (900–1000 °C), based on an yttria-stabilized zirconia (YSZ) electrolyte, a strontium-doped lanthanum manganate cathode, and an Ni-YSZ anode, have been developed extensively [1–4]. In view of increasing cell lifetime and the reduction of materials and operation costs, continuous effort has been devoted to the development of SOFCs working at intermediate temperatures (600–800 °C). Correspondingly, novel SOFC materials have been investigated in order to ensure satisfactory electrochemical performance for the cells at the reduced temperatures. $Ce_{0.8}Sm_{0.2}O_{1.9}$ (SDC) is a promising candidate for the electrolyte constituent of SOFCs, because of its superior oxygen ion conductivity at intermediate temperatures [5,6]. Ni-SDC cermet is selected as an anode due to its favorable electrocatalytic properties for fuel oxidation. $La_{0.6}Sr_{0.4}Co_{0.2}Fe_{0.8}O_{3-\delta}$ (LSCF) electron-ion mixed conductor shows great potential as a cathode of SOFCs for its extended triple-phase boundary and high catalytic activity at intermediate temperatures [7–9].

Over the past few decades, various structure designs of SOFC single cells have been developed, among which planar and tubular geometries are two most popular ones. Planar SOFCs show advantages of high volumetric power density and easy stacking. Whereas such single cells are prone to cracking due to

* Corresponding author. Tel.: +82 63 2702380; fax: +82 63 2702386.
E-mail address: kimbh@jbnu.ac.kr (B.-H. Kim).

0378-7753/$ – see front matter © 2013 Elsevier B.V. All rights reserved.
http://dx.doi.org/10.1016/j.jpowsour.2013.07.022

the restriction of thermal expansion by the configuration. In addition, a large sealing area makes the design less desirable [10,11]. Tubular SOFCs show merits of reduced sealing area and high mechanical strength [12,13]. They could endure rapid start-up and shut-down cycles, which is a significant practical advantage.

Generally, tubular SOFCs are categorized as cathode-supported, electrolyte-supported and anode-supported structures, with Ni-containing anode-supported ones being considered as the representative because of their high electrocatalytic activities. Ni-containing supporters, however, suffer from poor redox cycling stability due to volume changes arising from the reduction and oxidation of nickel [14–16]. This problem leads to the formation of cracks in the electrolyte layer and, as a result, a performance degradation or even failure of the single cell.

To improve the redox cycling stability of the single cell, we designed an inert-substrate-supported tubular cell with a configuration of porous YSZ supporter/Ni anode current collector/Ni-SDC anode/YSZ/SDC bi-layer electrolyte/LSCF cathode. The rigid porous YSZ supporter improves the mechanical strength and reduces the dimensional change upon anode reoxidation. Meanwhile, the porous YSZ supporter inhibits the propagation of delamination in the anode, thus improving the bulk volume stability of the single cell [17]. These functions may pave the way to solving the redox cycling stability problem of tubular SOFCs.

Furthermore, the adoption of Ni anode current collector and Ni-SDC anode layers integrates the high conductivity of Ni and excellent electrocatalytic activity of Ni-SDC anode for fuel oxidation, allowing an enhanced performance of the single cell. YSZ/SDC bi-layer electrolyte prevents the chemical reaction between LSCF cathode and YSZ electrolyte and formation of poor conducting phases (e.g., $La_2Zr_2O_7$ and $SrZrO_3$) [18]. In addition, the SDC layer facilitates cathode electrochemical reaction and improves the electrochemical performance of the single cell [19,20]. In another aspect, the chemical reaction has been identified at the interface between YSZ and SDC layers when fabricating the single cells by co-sintering process. The thickness of $(SDC)_x(YSZ)_{1-x}$ solid solutions have been determined to be 1.6 μm in our previous research [21]. As the conductivities of the $(SDC)_x(YSZ)_{1-x}$ solid solutions are similar to pure YSZ, they could not significantly affect the performance of the single cells with YSZ as electrolyte [22].

To realize the functions of the inert substrate, the YSZ supporter should have sufficient porosity to ensure the diffusion of fuel gas. One the other hand, a reasonable mechanical strength is needed to support the whole single cell. Hence, a balance between the two requirements appears as an important issue. Efforts on this issue would provide a technological base for the development of inert-substrate-supported single cell.

In this work, we fabricated the inert-substrate-supported single cells by a cold isostatic pressing and dip-coating process. Poly (methyl methacrylate) (PMMA) was employed to tailor the porosity of the YSZ supporter. The mechanical strength and electrochemical performance of the single cells were investigated as a function of the amount of the pore former. Moreover, the redox cycling stability of the single cells was examined.

2. Experimental

2.1. Powder preparation

SDC powder and NiO-SDC powder containing 61.3 wt.% NiO were synthesized by urea combustion. LSCF powder was synthesized by glycine-nitrate combustion. The details of powder synthesis have been reported previously [23–25].

2.2. Preparation of porous YSZ tubular supporter

YSZ (TZ-8Y) powder was mixed with PMMA (S50, Sunjin Chemical) pore former at weight percentage values of 10, 15, 20, 25, and 30 wt.%, respectively, by ball milling in ethanol for 24 h. The YSZ supporters were denoted as YSZ (x) (with the amount of PMMA x = 10–30 wt.%). 5 wt.% polyvinyl alcohol solution was added to the mixed powders as a binder. The powders were filled into the cavity between a metallic mandrel and rubber mold and compressed into tubes at 100 MPa using a cold isostatic press (CL4-22-60, Nikkiso). The length of the green tubes was 85 mm, while the inner and outer diameters were 4 and 11 mm, respectively. After polishing to an outer diameter of 6 mm, the tubes were calcined at 1000 °C for 3 h in air to ensure adequate strength of the supporters.

2.3. Fabrication of the single cell

16 wt.% NiO and 1.8 wt.% PMMA powders were mixed with a lab-made organic carrier (I) to form a slurry for the anode current collector. The organic carrier (I) was composed of 48 wt.% 2-butanone (Samchun Chemicals), 48 wt.% ethanol (Hayman Specialty Products), 0.5 wt.% triethanolamine (Samchun Chemicals), 1.0 wt.% dibutyl phthalate (Aldrich), 1.0 wt.% polyethylene glycol 300 (Showa Chemical), and 1.5 wt.% Butvar B-98 (Sigma). NiO layer was deposited on the outer surface of the YSZ supporters by a dip-coating process. To prevent the formation of cracks and pin-holes during sintering due to the evaporation of organics, the NiO layer was dried in air for 12 h and then calcined at 600 °C for 1 h.

16 wt.% NiO-SDC and 1.8 wt.% PMMA powders were mixed with the organic carrier (I) to form a slurry for the anode. The NiO-SDC was coated onto the surface of the NiO layer via the same dip-coating process. The samples were heated at 1000 °C to adjust the shrinkage behavior in the sintering process.

17 wt.% YSZ powder was mixed with lab-made organic slurry (II) by ball-milling for 24 h. The organic slurry (II) comprised 40 wt.% α-terpineol (Kanto Chemical Co. Inc), 30 wt.% B73210 organic binder (Ferro Electronics Materials), and 30 wt.% ethanol. The YSZ layer was deposited on the surface of the NiO-SDC layer via the dip-coating process. The SDC layer was fabricated on the surface of the YSZ layer using the same process. The samples were then co-sintered at 1400 °C for 4 h in air.

Finally, the LSCF cathode with a surface area of 1.41 cm^2 was coated onto the surface of the electrolyte by a spraying method. 14 wt.% LSCF powder was mixed with organic slurry (III) containing 1 wt.% ethyl cellulose (Showa Chemical) and 99 wt.% ethanol by ball-milling for 24 h to obtain a cathode ink. The ink was sprayed onto the SDC surface driven by 1 atm air as a carrier gas. The tube was rotated at a constant speed using an electric motor during the spraying process. The cathode was sintered at 950 °C for 2 h in air.

2.4. Structure characterization

The porosity of the YSZ supporter was examined using a porosimeter (AutoPore IV 9500, Micromeritics). The mechanical strength of the cell was determined by the three-point bending method using a universal testing machine (LR5K-plus, Lloyd Instruments) [26]. The microstructure of the cell was investigated by a scanning electron microscope (SEM, JSM-6400, JEOL). The thicknesses of the Ni and Ni-SDC layers were determined by an energy-dispersive X-ray spectroscopy line scan (EDX, APOLLO X). The thicknesses of the LSCF, SDC, and YSZ layers, and the pore size distribution in the YSZ supporter were estimated using an image analysis method with the aid of Image-Pro Plus 6.0 software [27].

2.5. Electrical resistance

A four-probe method was used to measure the sheet resistance of the Ni layer on the porous YSZ supporter in hydrogen (shown in Fig. 1). The sheet resistance (R_s) was calculated using the following equation [28]:

$$R_s = R\cdot(\pi\cdot D)/L \quad (1)$$

where R is the resistance between A and B, D is the outer diameter of the tube, and L is the distance between A and B.

2.6. Cell performance measurement

The performance of the tubular single cell was investigated using a custom-built testing system assembled with a gas flow controller (FM-30VE, Line Tech), a temperature controller, a sample holder (shown in Fig. 2), and an electrochemical work station (SP 150, Biologic SAS). Pt mesh and Pt wire were used as current collectors for the cathode, and Ni mesh and Ni wire were used as the current collectors for the anode. Glass binder was used as a gas-tight seal. The cell was first heated to 900 °C and held there for 15 min to ensure good sealing by the glass, and then cooled down to 800 °C. During the heating and cooling processes, nitrogen (200 ml min^{-1}) was used as a shielding gas to prevent oxidation of the Ni mesh and Ni wire at the anode. After the temperature reached 800 °C, hydrogen was fed into the anode side at 200 ml min^{-1} to reduce the anode, and the cathode was exposed to air. The performance was tested by the four-probe method. Electrochemical impedance spectra (EIS) of the single cell were obtained in potentiostatic and galvanostatic modes, respectively, over a frequency range of 0.01 Hz–100 kHz. In potentiostatic mode, the EIS were measured under open-circuit voltage (OCV) condition and the amplitude of the input sinuous signal was 10 mV. In galvanostatic mode, the current density passing through the cell was increased from 50 to 1300 mA cm^{-2} step by step and a 20 mA sinusoidal current signal was applied to the cell.

Redox cycling stability of the YSZ (25 wt.%) single cell was measured by alternating the supply of hydrogen, nitrogen and air to the anode. For each redox cycle, four steps were involved. In the first step, the anode was reduced in hydrogen until the OCV values of the single cell reached a steady state. Then, the cell voltage was measured at a current density of 300 mA cm^{-2} for 30 min in hydrogen. Afterward, the anode gas was changed to nitrogen for 10 min. Finally, the anode was exposed to air for 10 min. After nine redox cycles, performance stability of the single cell was investigated in hydrogen at the current density of 300 mA cm^{-2} for 6 h.

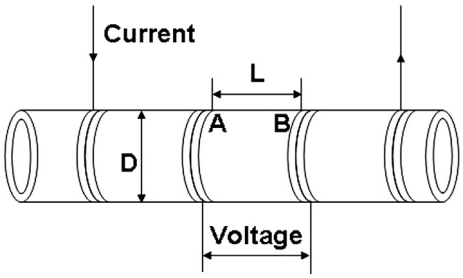

Fig. 1. Schematic diagram of sheet resistance measurement setup.

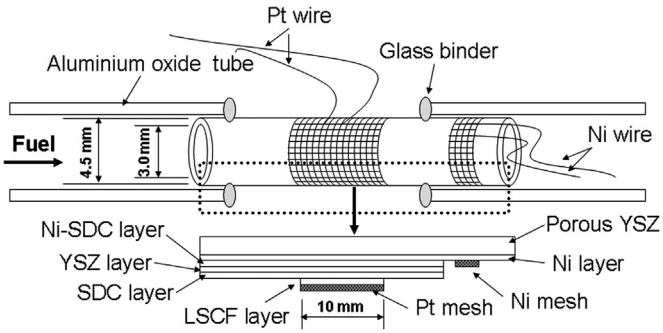

Fig. 2. Schematic diagram of tubular single cell and sample holder.

3. Results and discussion

3.1. Structure characterization

The pore morphology of the YSZ supporters has been analyzed by SEM images obtained from different parts of the supporters. A typical cross-sectional SEM image of the YSZ (25 wt.%) supporter is shown in Fig. 3a. The pore size distribution generally agrees with a Gaussian fitting (Fig. 3b). The data in Fig. 3c shows the average pore sizes and porosities of YSZ supporters with different amounts of PMMA pore former. Upon elevating the amount of PMMA from 10 to 15 wt.%, the average pore sizes show an evident increase from 1.2 ± 0.15 to 2.0 ± 0.15 μm, and the porosities exhibit a corresponding increase of about two-fold, from 13% to 30%. Increasing the PMMA amount further beyond 15 wt.% leads to linear improvements in the average pore sizes and porosities of the supporters. It is noted that excessively large pore size and porosity of YSZ supporter are unfavorable for the mechanical strength of the single cells (insert in Fig. 3c). Considering a minimum porosity requirement of 20% for gas flow in the electrode and required bending strength of 20 MPa, 15–25 wt.% PMMA are used to fabricate the YSZ supported single cell [26,29–31].

Typical cross-sectional SEM images of the single cell with the YSZ (25 wt.%) supporter are shown in Fig. 4. The thicknesses of the LSCF (10 μm), SDC (8 μm), and YSZ (25 μm) layers are estimated by an image analysis method. The thicknesses of the Ni-SDC and Ni layers are determined to be 12 and 15 μm by EDX line scan. Higher-magnification images (Fig. 4b and c) show good adhesions between the different layers. The LSCF cathode displays porous feature and good connection between nano-sized grains. The SDC and YSZ bilayer electrolyte appears dense with a few isolated pores. The Ni-SDC and Ni layers exhibit porous microstructure features with uniform distributions of micro-sized pores. In general, the thickness of the Ni layer increases with the amount of PMMA in YSZ supporters (insert in Fig. 4a), and all other layers show similar microstructure features.

3.2. Performance of the tubular single cell

The sheet resistances of the Ni layers on the porous YSZ supporters have been investigated (Fig. 5). A monotonous increase in sheet resistance is observed when increasing the temperature from 500 to 800 °C. This phenomenon could be attributed to the characteristics of metallic conductors [32]. At an identical measurement temperature, the sheet resistances decrease with increasing PMMA amount in the YSZ supporters. This could be ascribed to the increased thickness of the Ni layer. Increasing the PMMA amount enhances the porosity of the YSZ supporter, and more slurry is thus absorbed on the YSZ surface by capillary force, leading to improved

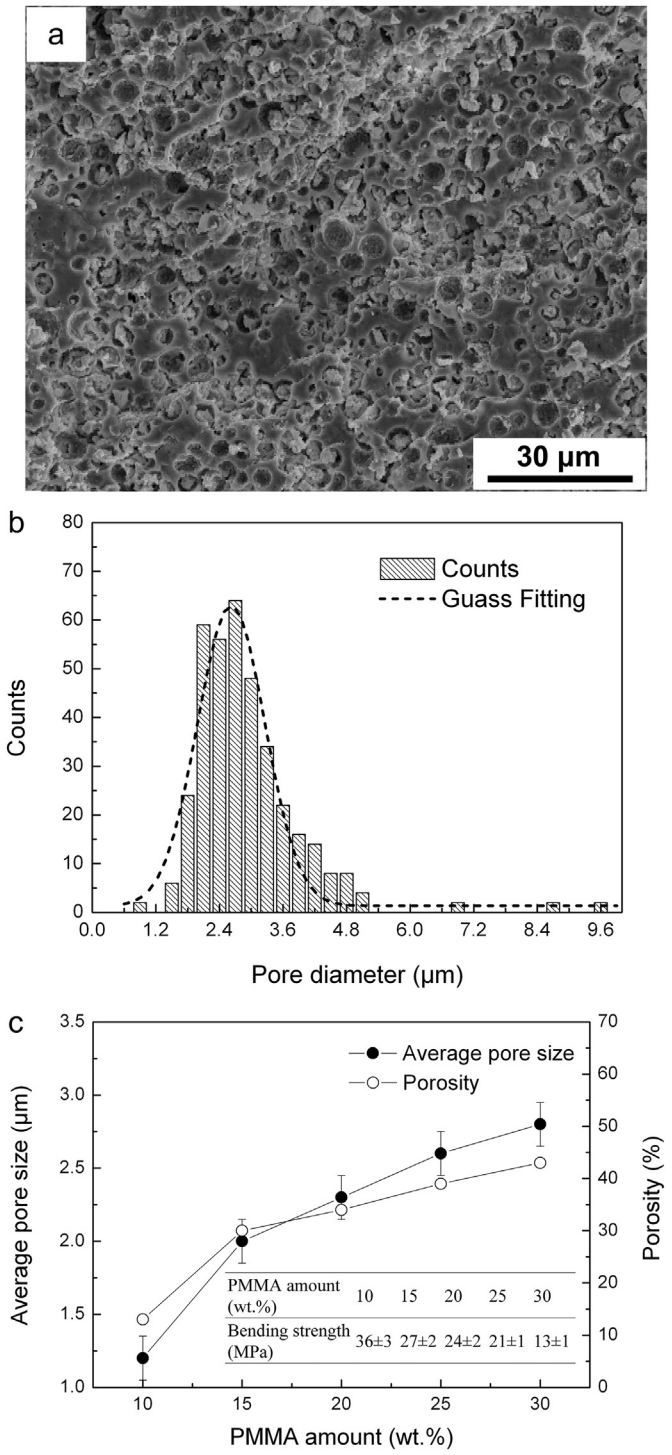

Fig. 3. (a) Cross-sectional SEM image of YSZ (25 wt.%), (b) pore size distribution in YSZ (25 wt.%) and (c) average pore sizes and porosities of YSZ supporters with different PMMA amount. The bending strengths of the single cells are inserted in (c).

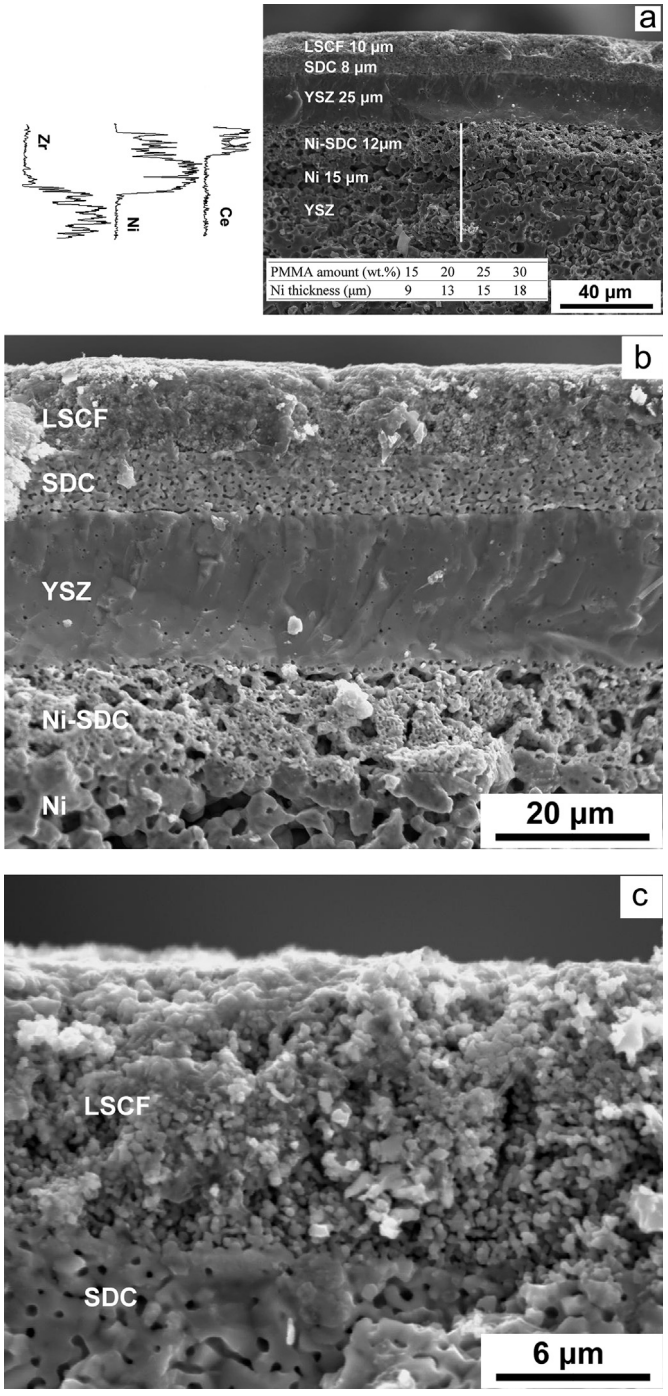

Fig. 4. Typical cross-sectional SEM image of the tubular single cell (a) low magnified image with EDX line scan, (b) and (c) high magnified images. Thicknesses of Ni layers with different PMMA amount in YSZ supporters are inserted in (a).

thickness of the Ni layer (insert in Fig. 4a) [33,34]. Additionally, higher PMMA content leads to larger shrinkage of the YSZ supporter in sintering process (insert in Fig. 5), resulting in improved connection between Ni grains. Therefore, the sheet resistance of Ni layer is reduced.

The data in Fig. 6 shows the voltages and power densities of the cells as a function of current densities at 800 °C. The OCV values of each cell are around 1.10 V, close to the theoretically predicted value, indicating a dense YSZ/SDC bi-layer electrolyte and good sealing by the glass to prevent gas leakage [35]. The maximum power densities of the cells improve as the PMMA amount increases from 15 to 25 wt.%. The cell with the YSZ (25 wt.%) supporter exhibits an optimum maximum power density of 337 mW cm^{-2}. The performance of the cell is similar to Ni-YSZ anode-supported tubular single cell fabricated by the phase inversion and vacuum assisted coating techniques (377 mW cm^{-2}, at 800 °C in humidified hydrogen) [36]. On the other hand, the performance is competitive as compared to the Ni-YSZ-anode-supported tubular single cell (62 mW cm^{-2}, at

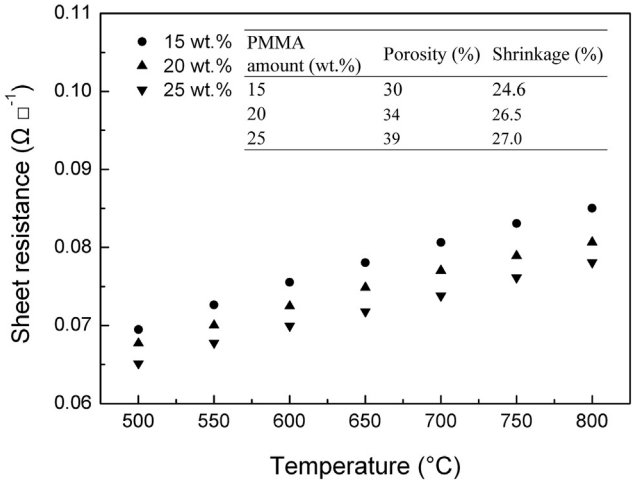

PMMA amount (wt.%)	Porosity (%)	Shrinkage (%)
15	30	24.6
20	34	26.5
25	39	27.0

Fig. 5. Sheet resistances of the Ni layers with different PMMA amount in YSZ supporters. The insert shows the porosities and shrinkages of the YSZ supporters.

900 °C in humidified hydrogen) fabricated by a similar isostatic pressing method [37].

The EIS of the single cells are obtained under OCV conditions in hydrogen. The Nyquist plots are shown in Fig. 7. The impedance spectra are fitted according to an $LR_{ohm}(R_1Q_1)(R_2Q_2)$ equivalent circuit model. L is an inductance element representing the impedance response caused by the measurement device and connecting wires. R_{ohm} is the ohmic resistance of the single cell, and (RQ) components correspond to the involved electrode processes, where R is the resistance, and Q is the constant phase element. The equivalent capacitance C and relaxation frequency f of an electrode process corresponding to a specific (RQ) component can be calculated according to the following equations [38]:

$$C = (R\cdot Q)^{1/n}/R \tag{2}$$

$$f = (R\cdot Q)^{-1/n}/(2\pi) \tag{3}$$

where n is an exponent, which can be obtained by the EIS fitting. The constant phase element Q represents an ideal capacitor and an ideal resistor when $n = 1$ and $n = 0$, respectively. When $0 < n < 1$, the circuit element reflects inhomogeneity of the electrode system.

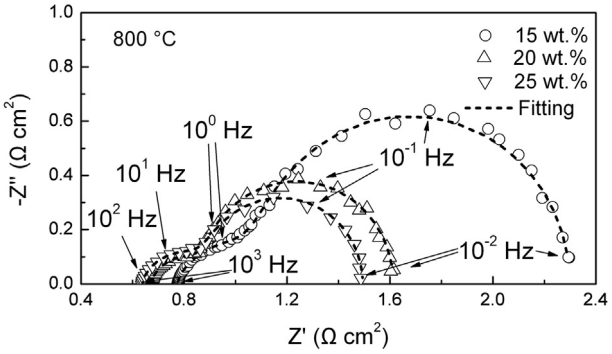

Fig. 7. Nyquist plots of the tubular single cells with different PMMA amount in YSZ supporters measured at 800 °C under OCV condition in hydrogen.

The equivalent capacitance and relaxation frequency can be regarded as characteristic parameters to identify electrochemical processes. The electrochemical process corresponding to the component (R_1Q_1) has the equivalent capacitance of 10^{-2} F cm^{-2} and the relaxation frequency of 10^0–10^1 Hz, respectively. They are in the typical range for the electrode process. The equivalent capacitance and relaxation frequency for (R_2Q_2) component are on the orders of magnitude of 10^0 F cm^{-2} and 10^{-1} Hz, respectively. This process is assigned to gas diffusion process [38–42].

Electrochemical parameters derived from the impedance spectra fitting are shown in Fig. 8. Given similar microstructure features of the cathodes, electrolytes, and anodes, the variations in the electrochemical parameters can be attributed to the differences in the Ni anode current collectors and porous YSZ supporters. At 800 °C, R_{ohm} decreases with the increase in the amount of PMMA. This behavior is presumed to originate from the variation in the sheet resistance of the Ni layer. As shown in Fig. 5, the sheet resistance of the Ni layer decreases with increases in the amount of PMMA in the YSZ supporter, thus reducing R_{ohm} of the single cell.

The polarization resistances of the single cells exhibit an evident decrease with the amount of PMMA. For each single cell, R_2 is apparently larger than R_1, implying a major contribution of gas diffusion process to overall electrode polarization. Moreover, R_2 values decrease with the amount of PMMA, suggesting an effect of

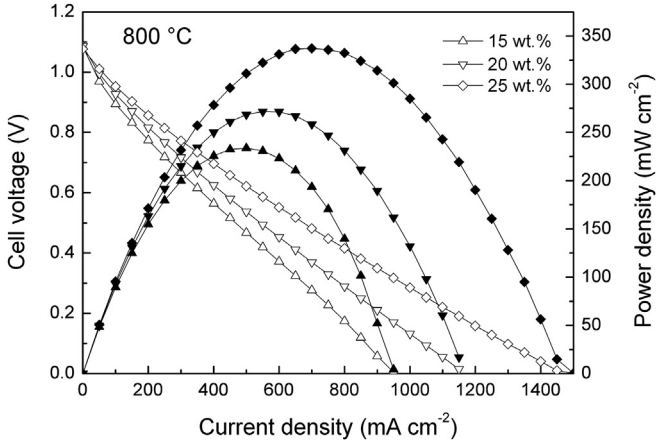

Fig. 6. Voltages and power densities of tubular single cells with different PMMA amount in YSZ supporters measured at 800 °C in hydrogen.

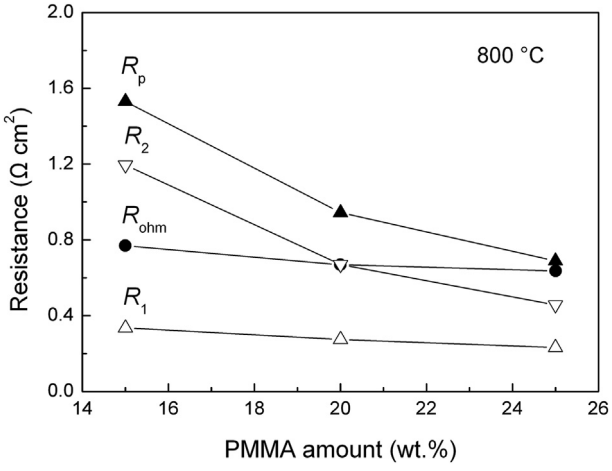

Fig. 8. Electrochemical parameters derived from EIS measured at 800 °C under OCV condition.

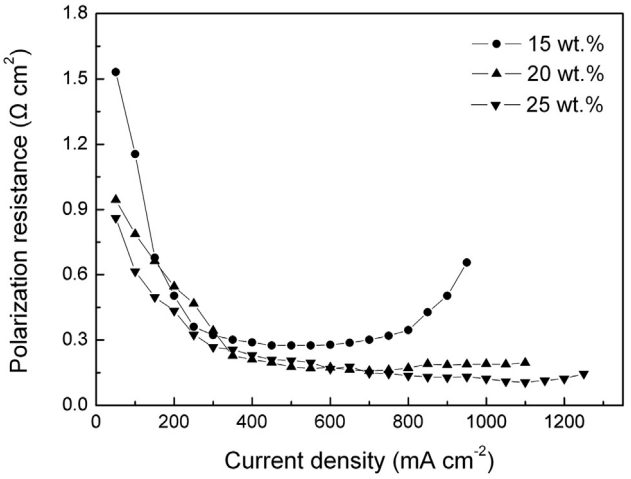

Fig. 9. Polarization resistances of the single cell with different PMMA amount in YSZ supporters measured at different current densities at 800 °C.

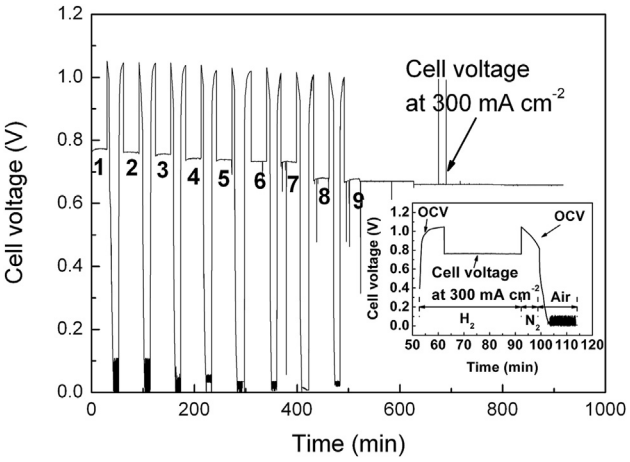

Fig. 10. Cell voltages in different redox cycles. The insert shows the schedule for each redox cycle.

microstructure of pores in YSZ supporter on the anode electrochemical reaction. Large pore size and high porosity in the YSZ supporter facilitate the gas diffusion process at the anode, which lowers the polarization resistance of the single cell.

The above findings can be further substantiated by the variation of the polarization resistances of the single cells at various current densities. Fig. 9 shows the polarization resistances of the single cells derived from EIS obtained under different current densities. In the low-current density range (<400 mA cm^{-2}), polarization resistances of the single cells decrease with increasing current density. This could be ascribed to the activation effect on the electrochemical reactions at the electrodes [43,44]. Whereas in the high current-density range (>400 mA cm^{-2}), the cell with low PMMA content (15 wt.%) shows increased polarization resistances with current densities. This reveals an effect of the pore size and porosity of the YSZ supporter on the anode electrode processes. Small pore size and low porosity in the YSZ supporter are unfavorable for the gas diffusion process at the anode, which increase the polarization resistance at high current densities. Increasing the pore size and porosity by higher PMMA loading (≥20 wt.%) facilitates the gas diffusion process, and therefore, the polarization resistances maintain the same value in the high current-density range as in the low current-density range.

3.3. Redox cycling stability

Redox cycling performance of the YSZ (25 wt.%) single cell is shown in Fig. 10. The schedule for each redox cycle is inserted in Fig. 10. Within seven redox cycles, the cell maintains 95% of its initial performance. After nine redox cycles, the performance is decayed by 13%. This could be due to the delamination in Ni anode current collector. Repetitive redox cycles lead to the formation of microcracks in Ni layer (shown in Fig. 11b), resulting in decreased performance of the single cell. On the other hand, the single cell exhibits significantly improved performance compared with the Ni-YSZ anode supported tubular single cell (performance degradation of 16% after one redox cycle at 800 °C) [45]. This is in agreement with the results of mechanical modeling for Ni-containing anode supporters in the redox process [17]. The propagation of the delamination in Ni layer could be suppressed by porous YSZ supporter, reducing the strain in YSZ electrolyte layer and improving the redox cycling stability of the single cell.

In addition, after nine redox cycles, the single cell shows good performance stability at 300 mA cm^{-2} in hydrogen for 6 h. In general, the single cell displays reasonably good redox cycling stability, highlighting the advantage of the tubular configuration described in the present work.

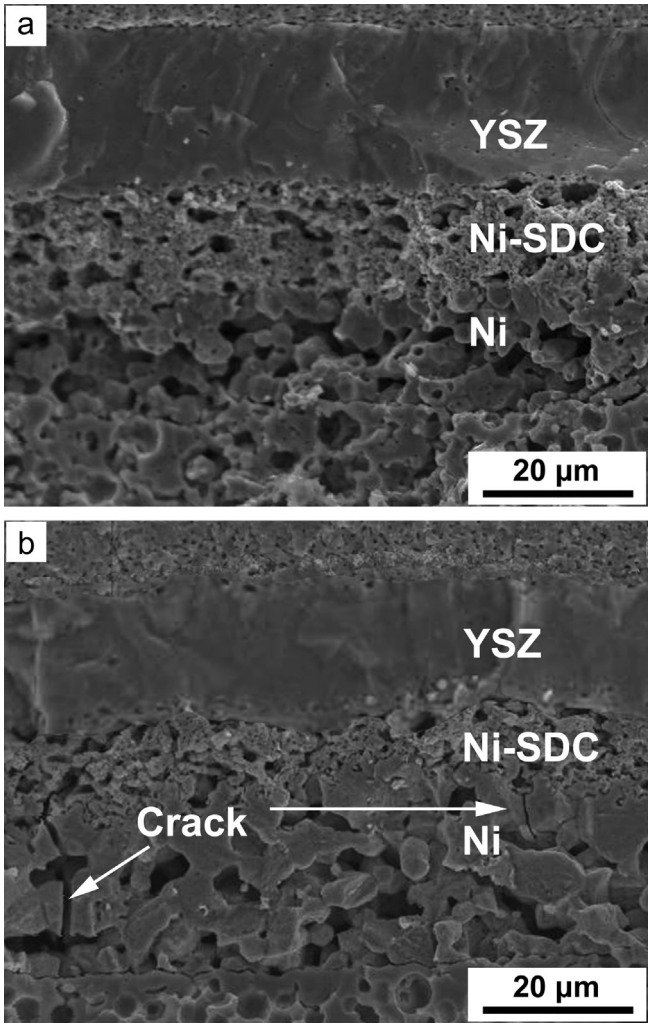

Fig. 11. Cross-sectional SEM image of the single cell: (a) after reduction in hydrogen, (b) after performance stability measurement.

4. Conclusions

A porous YSZ inert-substrate-supported tubular single cell has been fabricated by the cold isostatic pressing and dip-coating method. The microstructure feature, mechanical strength and electrochemical performance of the single cell have been investigated with respect to the amount of PMMA pore former in the YSZ supporter. The average pore size and porosity of the YSZ supporter increase with the amount of PMMA, facilitating the gas diffusion process at the anode and reducing the polarization resistance of the electrodes whereas resulting in a lowering of the mechanical strength of the single cell. The optimum PMMA content in YSZ supporter is determined to be 25 wt.%. The single cell with 25 wt.% PMMA in YSZ supporter shows a bending strength of 21 $\pm$ 1 MPa and a maximum power density of 337 mW cm^{-2} at 800 °C in hydrogen. Moreover, the inert-substrate-supported tubular single cell exhibits an excellent redox cycling stability, maintaining 95% of its initial performance within seven redox cycles. The results of the present work highlight the advantages of the inert-substrate-supported configuration in improving redox cycling stability of tubular single cell.

Acknowledgments

This research is a result of the study on the “Leades Industry-University Cooperation” Project, supported by the Ministry of Education, Science & Technology (MEST) and the Human Resources Development of KETEP (No. 20114030200060), funded by the Korea government Ministry of Knowledge Economy. This work was also supported by Hubei Provincial Science and Technology Department (No. 2012IHA01001).

References

[1] E. Tsipis, V. Kharton, J. Solid State Electrochem. 12 (2008) 1039–1060.
[2] X.J. Chen, K.A. Khor, S.H. Chan, L.G. Yu, Mater. Sci. Eng. A 335 (2002) 246–252.
[3] V.A.C. Haanappel, J. Mertens, D. Rutenbeck, C. Tropartz, W. Herzhof, D. Sebold, F. Tietz, J. Power Sources 141 (2005) 216–226.
[4] W.Z. Zhu, S.C. Deevi, Mater. Sci. Eng. A 362 (2003) 228–239.
[5] V.V. Kharton, F.M.B. Marques, A. Atkinson, Solid State Ionics 174 (2004) 135–149.
[6] S. Hui, J. Roller, S. Yick, X. Zhang, C. Decès-Petit, Y. Xie, R. Maric, D. Ghosh, J. Power Sources 172 (2007) 493–502.
[7] A. Mineshige, J. Izutsu, M. Nakamura, K. Nigaki, J. Abe, M. Kobune, S. Fujii, T. Yazawa, Solid State Ionics 176 (2005) 1145–1149.
[8] A. Esquirol, N.P. Brandon, J.A. Kilner, M. Mogensen, J. Electrochem. Soc. 151 (2004) A1847–A1855.
[9] F. Tietz, V.A.C. Haanappel, A. Mai, J. Mertens, D. Stöver, J. Power Sources 156 (2006) 20–22.
[10] J.H. Myung, H.J. Ko, H.G. Park, M. Hwan, S.H. Hyun, Int. J. Hydrogen Energy 37 (2012) 498–504.
[11] M.K. Mahapatra, K. Lu, Mater. Sci. Eng. R 67 (2010) 65–85.
[12] N.M. Sammes, Y. Du, Int. J. Appl. Ceram. Tecnol. 4 (2007) 89–102.
[13] K. Kendall, Int. J. Appl. Ceram. Tecnol. 7 (2010) 1–9.
[14] D. Fouquet, A.C. Müller, A. Weber, E. Ivers-Tiffée, Ionics 9 (2003) 103–108.
[15] D. Waldbillig, A. Wood, D.G. Ivey, Solid State Ionics 176 (2005) 847–859.
[16] C.M. Dikwal, W. Bujalski, K. Kendall, J. Power Sources 181 (2008) 267–273.
[17] D. Sarantaridis, A. Atkinson, Fuel Cells 7 (2007) 246–258.
[18] W.H. Kim, H.S. Song, J. Moon, H.W. Lee, Solid State Ionics 177 (2006) 3211–3216.
[19] M. Chen, J.L. Luo, K.T. Chuang, A.R. Sanger, Electrochim. Acta 63 (2012) 277–286.
[20] M. Liu, D. Dong, R. Peng, J. Gao, J. Diwu, X. Liu, G. Meng, J. Power Sources 180 (2008) 215–220.
[21] M. Chen, B.H. Moon, S.H. Kim, B.H. Kim, Q. Xu, B.G. Ahn, Fuel Cells 12 (2012) 86–96.
[22] A. Martínez-Amesti, A. Larrañaga, L.M. Rodríguez-Martínez, M.L. Nó, J.L. Pizarro, A. Laresgoiti, M.I. Arriortua, J. Power Sources 192 (2009) 151–157.
[23] M. Chen, B.H. Kim, Q. Xu, B.K. Ahn, W.J. Kang, D.P. Huang, Ceram. Int. 35 (2009) 1335–1343.
[24] M. Chen, B.H. Kim, Q. Xu, O.J. Nam, J.H. Ko, J. Eur. Ceram. Soc. 28 (2008) 2947–2953.
[25] Q. Xu, D.P. Huang, W. Chen, F. Zhang, B.T. Wang, J. Alloy. Compd. 429 (2007) 34–39.
[26] N. Droushiotis, U. Doraswami, K. Kanawka, G.H. Kelsall, K. Li, Solid State Ionics 180 (2009) 1091–1099.
[27] B. Iwanschitz, L. Holzer, A. Mai, M. Schütze, Solid State Ionics 211 (2012) 69–73.
[28] R.N. Basu, S.K. Pratihar, M. Saha, H.S. Maiti, Mater. Lett. 32 (1997) 217–222.
[29] C.W. Tanner, K. Fung, A.V. Virkar, J. Electrochem. Soc. 144 (1997) 21–30.
[30] M.H.D. Othman, Z. Wu, N. Droushiotis, G. Kelsall, K. Li, J. Membr. Sci. 360 (2010) 410–417.
[31] L. Grahl-Madsen, P. Larsen, N. Bonanos, J. Engell, S. Linderoth, J. Mater. Sci. 41 (2006) 1097–1107.
[32] X. Fang, G. Zhu, C. Xia, X. Liu, G. Meng, Solid State Ionics 168 (2004) 31–36.
[33] M. Gaudon, C. Laberty-Robert, F. Ansart, P. Stevens, J. Eur. Ceram. Soc. 26 (2006) 3153–3160.
[34] H.J. Son, R.H. Song, T.H. Lim, S.B. Lee, S.H. Kim, D.R. Shin, J. Power Sources 195 (2010) 1779–1785.
[35] M. Henke, J. Kallo, K.A. Friedrich, W.G. Bessler, Fuel Cells 11 (2011) 581–591.
[36] C. Yang, W. Li, S. Zhang, L. Bi, R. Peng, C. Chen, W. Liu, J. Power Sources 187 (2009) 90–92.
[37] T. Mahata, S.R. Nair, R.K. Lenka, P.K. Sinha, Int. J. Hydrogen Energy 37 (2012) 3874–3882.
[38] D. Chen, R. Ran, K. Zhang, J. Wang, Z. Shao, J. Power Sources 188 (2009) 96–105.
[39] B. Morel, R. Roberge, S. Savoie, T.W. Napporn, M. Meunier, Appl. Catal. A 323 (2007) 181–187.
[40] V.C. Kournoutis, F. Tietz, S. Bebelis, Fuel Cells 9 (2009) 852–860.
[41] B. Iwanschitz, J. Sfeir, A. Mai, M. Schütze, J. Electrochem. Soc. 157 (2010) B269–B278.
[42] C. Fu, S.H. Chan, Q. Liu, X. Ge, G. Pasciak, Int. J. Hydrogen Energy 35 (2010) 301–307.
[43] X.D. Zhou, L.R. Pederson, J.W. Templeton, J.W. Stevenson, J. Electrochem. Soc. 157 (2010) B220–B227.
[44] J. Fleig, F.S. Baumann, V. Brichzin, H.R. Kim, J. Jamnik, G. Cristiani, H.U. Habermeier, J. Maier, Fuel Cells 6 (2006) 284–292.
[45] J. Pusz, A. Smirnova, A. Mohammadi, N.M. Sammes, J. Power Sources 163 (2007) 900–906.